Catal Lett (2018) 148:173–180
DOI 10.1007/s10562-017-2222-2

Palladium Nanoparticles Covered on Amine-Functionalized Mesoporous Hollow SiO_2 Spheres for the Reduction of 4-Nitrophenol

Xiang Liu[1,2] · Xiaohua Zhao[3] · Lei Zhu[1] · Ningning Liu[1] · Tian Tian[1]

Received: 26 June 2017 / Accepted: 11 October 2017 / Published online: 29 October 2017
© Springer Science+Business Media, LLC 2017

Abstract Highly dispersed Pd nanoparticles (NPs) covered on amine-functionalized mesoporous hollow SiO_2 spheres (Pd/MHSS-NH_2) have been successfully prepared. The morphology, structure and composition of Pd/MHSS-NH_2 were characterized by Transmission electron micrograph (TEM), N_2 ad-desorption, X-ray diffraction (XRD), Fourier-transfer infrared spectroscopy (FT-IR) and X-ray photoelectron spectroscopy (XPS). The as-prepared Pd/MHSS-NH_2 exhibited remarkably high activity for the reduction of 4-nitrophenol (4-NP) compared with other catalysts, which could be attributed to high dispersion of Pd NPs, amine functional groups on MHSS support, as well as mesoporous MHSS-NH_2 shell. Additional, the Pd/MHSS-NH_2 catalyst could be recovered by centrifugation from the reaction mixture and recycled six times without loss in activity.

Graphical Abstract

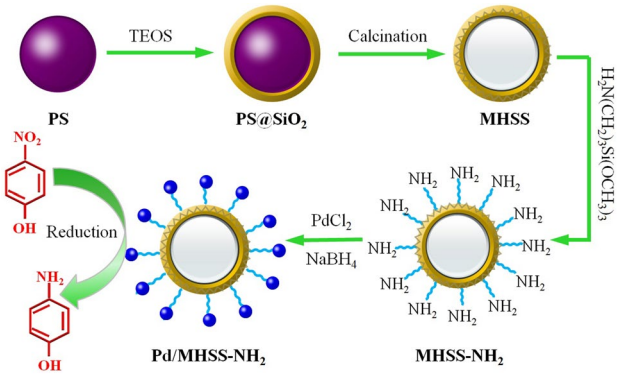

Keywords Pd nanoparticles · MHSS-NH_2 · 4-Nitrophenol reduction

1 Introduction

Palladium NPs have attracted considerable attentions because of their excellent catalytic properties and their practical application, such as C–C coupling reactions [1, 2], hydrogenation reactions [3] and oxidation reaction [4]. However, the agglomeration of Pd NPs is inevitable as a result of van der Walls forces [5]. In order to overcome this obstacle, a promising strategy has been made to immobilize Pd NPs on porous materials, such as zeolites [6], MOFs [7], polymers [8], etc.

In recent years, a special class of core–shell structures encapsulated Pd NPs has received increasing attention and has been widely applied in important catalytic reactions because of the following advantages: (I) the moveable core can expose more active sites to interact with the guest molecules more effectively; (II) the outer shells can prevent

Electronic supplementary material The online version of this article (doi:10.1007/s10562-017-2222-2) contains supplementary material, which is available to authorized users.

✉ Xiaohua Zhao
zhao12_19@163.com

[1] Zhenjiang Key Laboratory of Functional Chemistry & Institute of Medicine & Chemical Engineering, Zhenjiang College, Zhenjiang 212000, China

[2] Biofuels Institute of Jiangsu University, Zhenjiang 212013, China

[3] School of Materials Science and Engineering, Jiangsu University, Zhenjiang 212013, China

the aggregation of neighboring Pd NPs; (III) the hollow spaces between the cores and the shells can provide homogeneous micro-environment for the catalyst and reactants, which greatly improves the catalytic activity and stability [9–11]. Therefore, hollow porous structures incorporated with catalytically active cores have shown promise as nano reactors for catalysis. For example, Liao et al. reported Pd NPs loaded a mesoporous hollow silica sphere (Pd/MHSS) for phenol hydrogenation as an effective catalyst. However, the easy aggregation of MHSS results in a weak interaction between MHSS and Pd NPs, which decrease the utilization for Pd NPs storage [12]. Recently, N-modified silica spheres have been widely used for stabilizing ultra-small Pd NPs owing to nitrogen lead to enhanced interaction between an N-doped carbon material and Pd NPs [13–15]. For example, the PdAg/SiO_2-NH_2 catalyst, loading Pd and Ag NPs onto NH_2-modified SiO_2, was successfully prepared by professor Li's group. It was found that NH_2 functional group largely enhanced its catalytic nitrate reduction performance. In another work, Pd@SiO_2-NH_2 exhibited great activity and stability in the Cr(VI) reduction due to the coordination ability and electron-donating properties of NH_2 [16]. Hence, we prepared amine-functionalized mesoporous hollow SiO_2 spheres (MHSS-NH_2) as support material to load Pd NPs. As described in Scheme 1, MHSS were firstly prepared. Next, the MHSS-NH_2 was obtained successfully by coated with (3-aminopropyl)trimethoxysilane. Finally, $PdCl_2$ was supported on the surface of MHSS-NH_2, and the Pd(II) was reduced to Pd(0) NPs by $NaBH_4$. The catalytic properties of the resultant Pd/MHSS-NH_2 catalyst are evaluated by reduction of 4-nitrophenol as a model reaction. Furthermore, the reusability of Pd/MHSS-NH_2 catalyst was also investigated, which could be easily separated from reaction by centrifugation and recycled several times without obvious deterioration in catalytic activity.

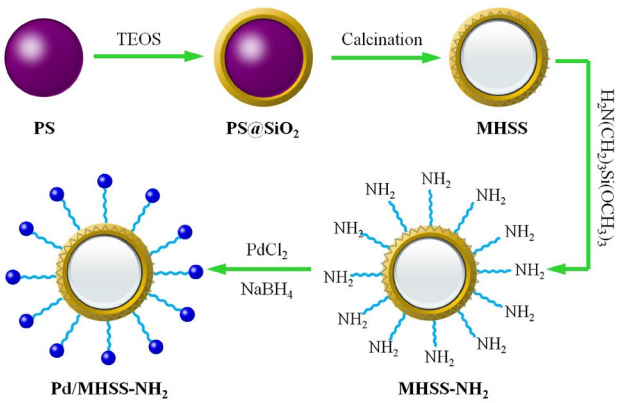

Scheme 1 Schematic illustration for the synthesis of Pd/MHSS-NH_2 catalyst

2 Experimental Details

2.1 Materials

(2-(Acryloyloxy)ethyl) trimethylammonium chloride (AETAC, 80 wt% in water), hexadecyltrimethylammonium bromide (CTAB, > 99.0%), 2,2′-azobis(2-methylpropionamidine) dihydrochloride (V-50, > 97.0%), (3-aminopropyl) triethoxylsilane (APS), styrene and tetraethyl orthosilicate (TEOS) were purchased from Aldrich without further purification.

2.2 Preparation of Mesoporous Hollow SiO_2 Spheres (MHSS)

The mesoporous hollow SiO_2 spheres were synthesized according to the literature with some modification [17]. To prepare the polystyrene, 1.0 g of AETAC (80 wt% in H_2O) was dissolved in 390.0 g water in a 500 mL round-bottom flask. 40.0 g styrene was added slowly to the solution and kept stirring at 800 rpm by mechanical raking for 30 min. The mixture was purged with nitrogen for 20 min and then heated to 90 °C with an oil bath. Afterwards, 10 mL of an aqueous solution containing 1.0 g V-50 was added. The emulsion was kept at 90 °C for 24 h under nitrogen to complete the polymerization.

0.8 g of CTAB was dissolved in a mixture of 29.0 g of water, 12.0 g of ethanol and 1.0 mL of ammonium hydroxide solution. 10 mL polystyrene solution was added dropwise to the above CTAB solution at room temperature under vigorous stirring, followed by sonication for 10 min. The derived milky mixture was then magnetically stirred for 30 min before adding dropwise 4.0 g of TEOS. The mixture was kept stirring at room temperature for 48 h before the silica coated latex was harvested by centrifugation at 7000 rpm for 40 min. The precipitate was washed with copious amounts of ethanol and then dried at room temperature. Finally the material was calcined in air at 600 °C for 8 h using a heating rate of 5 °C/min.

2.3 Preparation of Amine-Functionalized Mesoporous Hollow SiO_2 Spheres (MHSS-NH_2)

Briefly, 1.0 g MHSS samples were dispersed in 80 mL ethanol solution, then, 2.5 g (3-aminopropyl)trimethoxysilane (APS) was dropped into the system. The mixture was refluxed for 24 h. After filtration, washing and drying, the amine-functionalized MHSS was obtained and denoted as MHSS-NH_2.

2.4 Preparation of Pd NPs Loaded Amine-Functionalized Mesoporous Hollow SiO_2 Spheres (Pd/MHSS-NH_2)

Pd/MHSS-NH_2 was synthesized by a conventional impregnation-reduction method. Typically, 400 mg of MHSS-NH_2 was dispersed in a 50 mL ethanol solution under ultrasonication for 30 min. Then 0.03 mmol of a $PdCl_2$ aqueous solution was added into the above solution. After ultrasonic treatment for 10 min, a freshly prepared and excess 0.01 M $NaBH_4$ aqueous solution was slowly dropped into the above mixture with vigorous stirring. After 120 min of reduction, the Pd/MHSS-NH_2 was obtained with the help of centrifugation. The product was washed thoroughly with deionized water and then dried in a vacuum at room temperature overnight.

2.5 Catalytic Experiments

The catalytic performance of the Pd/MHSS-NH_2 was investigated by the reduction of 4-NP to 4-AP with $NaBH_4$, which was monitored by UV–vis spectroscopy. Generally, the catalyst (10.0 mg of Pd/MHSS-NH_2 NPs) was mixed with excess $NaBH_4$, which were added into 50 mL of deionized water. Then, 2.5 mL of freshly prepared 4-NP aqueous solution (0.2 mM) was added into the above solution at room temperature. The color of the reaction solution changed from light yellow to dark yellow because of the formation of 4-AP. Checking the reaction progress was done by UV–vis spectra. For the recycling experiments, the catalyst was recovered by centrifugation, washed with water and EtOH, dried and reused.

2.6 Characterization

Transmission electron microscopy of the prepared samples was carried out using a beam voltage of 200 keV (JEOL-2010F). The samples were ultra-sonic dispersed in acetone and dropped on a 200-mesh holey carbon coated copper grid. The porosity characteristics of the samples were determined by N_2 physisorption performed at − 196 °C using static sorption procedures (NOVA 3000e). Samples were degassed at 200 °C under vacuum for 10 h prior to the experiments. The Brunauer–Emmett–Teller (BET) surface areas were calculated by linear part of the *t*-plot. Pore size distribution was estimated from the nitrogen adsorption isotherms using the Barrett–Joyner–Halenda (BJH) procedure [18]. The low-angle X-ray diffraction (XRD) was carried on a D8 ADVANCE diffractmeter using monochromatic Cu Kα radiation (40 kV, 200 mA). The diffraction counts were collected in the 2θ range 1°–10° at a scan speed of 1(°)·min^{-1}. And the high-angle XRD patterns was collected with a scanning speed of 8(°)·min^{-1} and a scanning step of 0.02° (Rigaku D/max-2200). Fourier Transform-Infrared (FT-IR) spectra were recorded with a Nicolet iS50 spectrometer in the wave number range of 4000–400 cm^{-1}. X-ray Photoelectron spectroscopy (XPS) data was collected on a ESCALA-B250Xi instrument, performed with C1s pesk (285 eV) as the reference. Inductively coupled plasma-optical emission spectrometer (ICP-OES) were performed on a VISTA-MPX spectrometer to measure the Pd content of the catalysts. The UV–vis absorption spectra were collected using a UV-2550 UV–vis spectrophotometer in the absorbance mode.

3 Results and Discussion

3.1 Recognition of the Catalyst

Morphology and particle size distribution studies were obtained with transmission electron microscope (TEM). TEM characterization of the synthesized MHSS-NH_2 and Pd/MHSS-NH_2 were shown in Fig. 1. Figure 1a, b showed TEM images of the obtained MHSS-NH_2 monodispersed particles with a uniform diameter of 210 nm. The TEM image confirmed the hollow structure of the resulting silica particles by calcination of resin-silica nanocomposite particles in air, in which the shells appear to be dark. The cross-linked shell could well prevent agglomeration after successful modification of MHSS with APS (MHSS-NH_2). The shell thickness of the cross-linked hollow sphere was approximately 35 nm. As shown in Fig. 1b, the shell possessed accessible mesoporous structure, which obtained through a cationic surfactant-assisted approach using CTAB as the structure-directing agent. The TEM images in Fig. 1c, d demonstrated that the Pd NPs had been successfully loaded onto the mesoporous hollow silica sphere without obvious change of the MHSS-NH_2 shell. Interestingly, the Pd NPs located exclusively on the surface of MHSS-NH_2. Barely any Pd NPs were observed separated from MHSS-NH_2 hollow spheres, because the nitrogen lone pair strongly coordinated with Pd NPs. Notably, the Pd/MHSS-NH_2 exhibited high dispersion of Pd NPs without aggregation. The Pd NPs had a narrow size range of 3–7 nm with the average particle size of 5.18 nm measured by TEM (inset of Fig. 2c), further confirming the uniform dispersion of Pd NPs.

The pore structure was further confirmed by the nitrogen adsorption–desorption isotherms, as shown in Fig. 2. Both MHSS-NH_2 and Pd/MHSS-NH_2 samples exhibited a typical type IV isotherm with apparent H4-type hysteresis loop and a sharp step at higher relative pressures, indicating the existence of mesoporous structure. The Brunauer–Emmett–Teller (BET) surface area of the MHSS-NH_2 were measured to be 310.68 m^2 g^{-1}. In comparison, the specific surface area of the Pd/MHSS-NH_2 was approximately 124.91 m^2 g^{-1} which was surprisingly less than MHSS-NH_2 due to the Pd NPs imbedding in the pore of the MHSS-NH_2. The

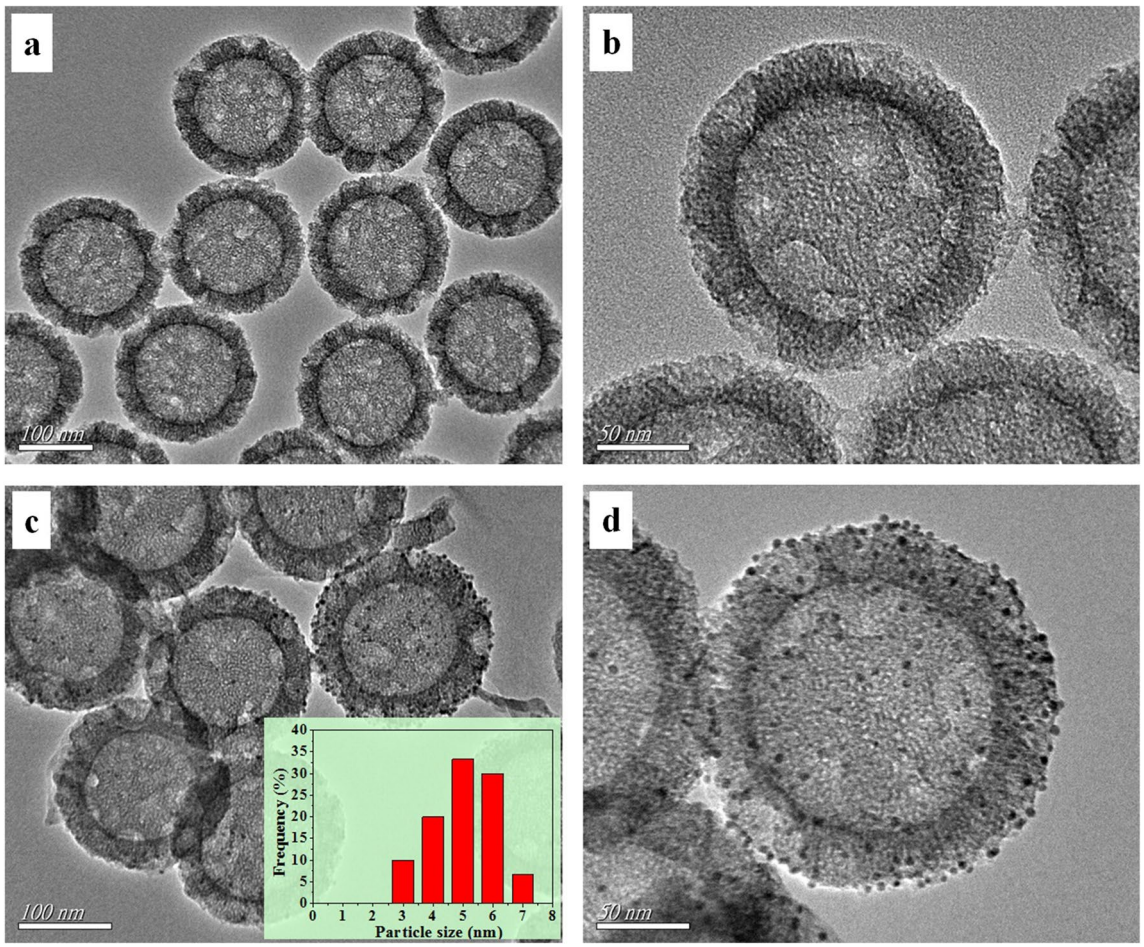

Fig. 1 TEM images of different mesoporous microspheres: **a, b** MHSS-NH_2 microspheres, **c, d** Pd/MHSS-NH_2 microspheres. The inset (**c**) displayed particle size distribution

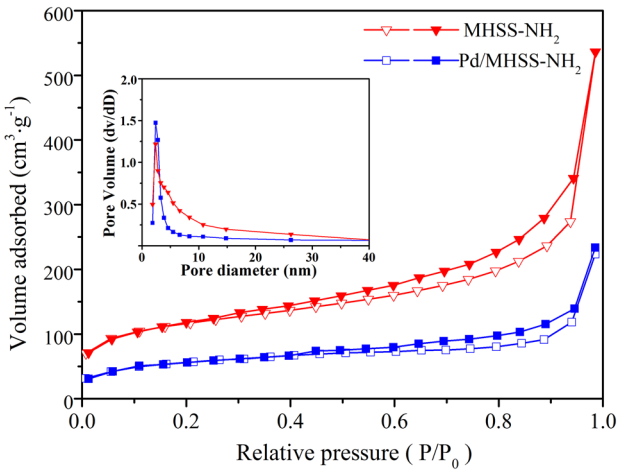

Fig. 2 Nitrogen adsorption–desorption isotherms and the corresponding BJH pore size distributions of MHSS-NH_2 and Pd/MHSS-NH_2 microspheres

Barrett–Joyner–Halenda (BJH) method was used to calculate the pore size distribution from deposition isotherm curves. The pore-size distribution of Pd/MHSS-NH_2 was about 2.7 nm in diameter, which was smaller than that of MHSS-NH_2 (5.99 nm). The smaller specific surface area and pore size distribution depicted that Pd NPs might partially occupied/blocked the mesoporous channels of MHSS-NH_2.

The low-angle and high-angle XRD patterns of MHSS-NH_2 and Pd/MHSS-NH_2 were shown in Fig. 3a, b, respectively. In both samples, a well-defined diffraction peak around $2\theta = 2°–4°$ was assigned to (100) diffraction peak of hexagonal mesoporous framework, which indicated the short-range ordered mesostructure of the synthesized MHSS-NH_2 and Pd/MHSS-NH_2. In addition, the (100) peak became weaker with addition of Pd NPs, indicating the decrease of mesoporous order. Obviously, the formation Pd NPs in the channel of mesopore could destruct the regularity of the mesophase. As observed in Fig. 3b, both samples exhibited a similar broad peak from 20° to 30° which can be ascribed to amorphous silica [19]. As for the sample Pd/

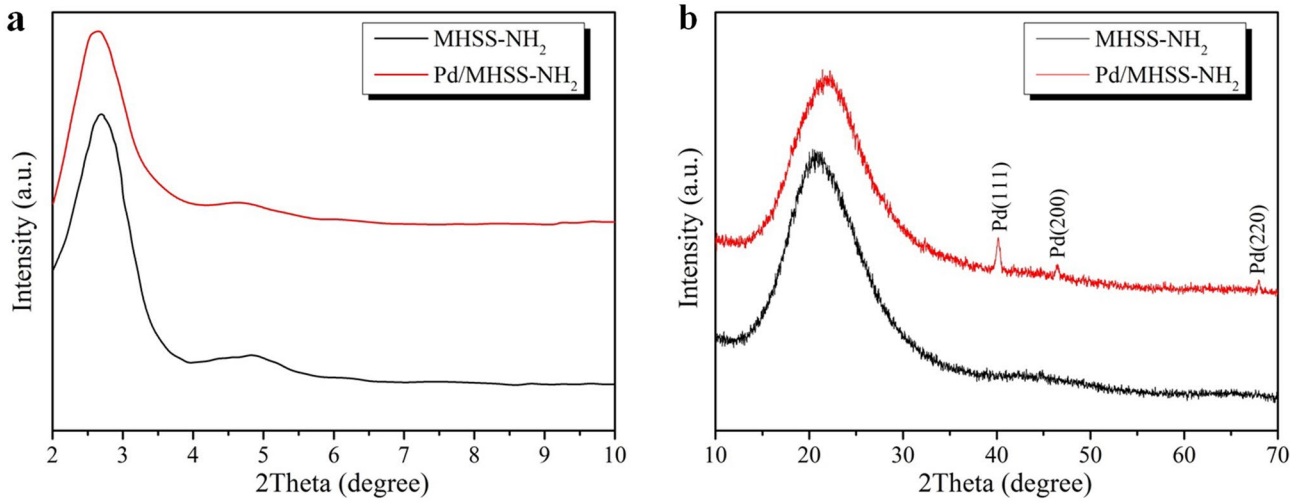

Fig. 3 The low (**a**) and high (**b**) angle XRD patterns of MHSS-NH_2 and Pd/MHSS-NH_2

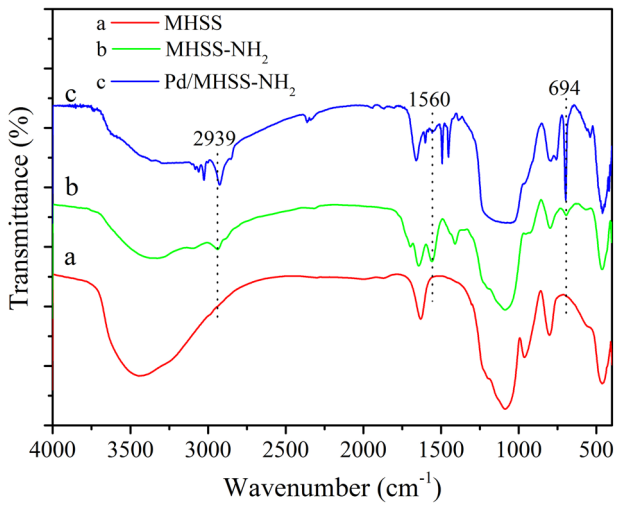

Fig. 4 The FT-IR spectra of MHSS, MHSS-NH_2 and Pd/MHSS-NH_2

MHSS-NH_2, three obvious new peaks at $2\theta = 40.2°$, 46.5° and 67.9° were indexed to (111), (200) and (220) diffraction planes of face-centered cubic Pd nanocrystals (JCPDS no. 05-0681), manifesting the formation of metallic palladium [20]. The XRD results implied that the Pd NPs had been successfully incorporated into the framework of mesoporous silica. Moreover, the average crystallite size calculated using Scherrer's equation is about 5.37 nm, which was in consistent with the average particle size observed in the TEM images.

The modification of MHSS with aminopropyl (MHSS-NH_2) was investigated by FT-IR. The FT-IR spectra of MHSS, MHSS-NH_2 and Pd/MHSS-NH_2 were shown in Fig. 4. The MHSS sample exhibited the characteristic bands at 1088, 962 and 802 cm^{-1}, which were attributed to Si–O–Si stretching vibration, SiO–H and Si–O–Si bending vibrations [21]. Besides, the Si–OH stretching vibration at 3444 cm^{-1} and bending vibration of physisorbed water (H–O–H) at 1632 cm^{-1} were clearly observed [22, 23]. After functionalizations, besides the same adsorption bands with MHSS, three new absorption peaks were clearly visible around 2939, 1560 and 694 cm^{-1}, which was a factor of the C–H stretching and bending vibration of amino-groups [24]. This confirmed the presence of amino-groups onto MHSS. In addition, peak intensity in the range of 3750–3000 cm^{-1} was reduced as a result of functionalizing MHSS with aminosilane groups. It's noteworthy that the characteristic bands of mesoporous silica and amino-groups were also observed in Pd/MHSS-NH_2, demonstrating the chemical stability of the MHSS-NH_2. The peaks at 1300–1500 and 3000–3200 cm^{-1} can be caused by the support of Pd NPs.

Figure 5a showed the representative survey XPS spectrum of Pd/MHSS-NH_2 catalyst, which clearly demonstrated the existence of Pd, Si, O, C, and N elements. In Fig. 5b, the Pd binding energy of Pd/MHSS-NH_2 exhibited two strong peaks centered at 340.5 and 335.2 eV, which were assigned to Pd $3d_{3/2}$ and Pd $3d_{5/2}$, respectively. These values agreed with the Pd(0) binding energy of Pd NPs. We found no oxidation state of Pd species, which indicated that Pd(II) would be reduced into Pd(0) completely, which was favorable to catalytic reduction reaction [25]. So the XPS analysis further identified the successful synthesis of Pd/MHSS-NH_2.

3.2 Catalytic Reduction of 4-Nitrophenol

As discussed above, the prepared Pd/MHSS-NH_2 exhibited hollow cavities and mesoporous structure shells, as well as Pd NPs densely attached on the surface of MHSS-NH_2. Therefore, Pd/MHSS-NH_2 microspheres would be an ideal

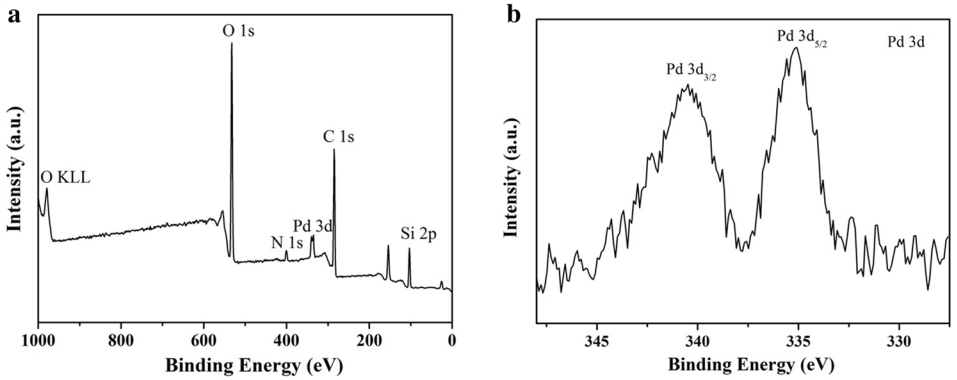

Fig. 5 **a** The survey X-ray photoelectron spectrum (XPS) of Pd/MHSS-NH_2 catalyst and **b** high resolution spectrum of Pd 3d

catalyst. In order to evaluate the catalytic performance of the Pd/MHSS-NH_2, the reduction of 4-NP was chosen as a model reaction in the presence of excess $NaBH_4$. As we known, 4-NP is a typical organic pollutant. On the other hand, the corresponding product (4-AP) is a familiar pharmaceutical intermediate [26, 27]. Hence, this catalytic reduction is always investigated to test the catalytic activity of Pd NPs. The reduction of 4-NP was detected by the UV–vis spectra. As shown in Fig. 6a, the catalytic process of 4-NP was failed in the absence of the Pd/MHSS-NH_2, which also confirmed the catalytic abilities of our as-prepared catalyst. 4-NP aqueous solution showed a strong absorption band at 400 nm when this reduction did not occur. After adding the Pd/MHSS-NH_2 NPs, the intensity of the absorption band at 400 nm gradually decreased resulting from the decreased 4-NP concentration. Meanwhile, a new and increased peak intensity appeared at 300 nm and which corresponding to the formation of 4-AP. The absorption peak at 400 nm disappeared after 8 min at room temperature, indicating a complete conversion of 4-NP into 4-AP.

For comparison, two sets of control experiments were carried out in the presence of Pd/MHSS and Pd/SiO_2-NH_2 catalysts, respectively (Fig. S1). Similarly, the absorption intensity at 400 nm became weaker along with the increasing reaction time, while the increase of absorption peak around 300 nm. Since the excess amount of $NaBH_4$, it could be inferred that the reaction rate was constant during reduction process, and the reaction could be considered as a pseudo first-order [28, 29]. So we calculated the corresponding pesudo first-order rate constant (K_{app}) from the linear relationship of $\ln(C/C_0)$ vs. reaction time, where the C and C_0 was evaluated using the peaks intensity at 400 nm. As shown in Table 1 and Fig. S2, the reaction rate constant (K_{app}) of Pd/MHSS-NH_2 was determined to be 0.006 s^{-1}, which was higher than that of Pd/MHSS (0.0043 s^{-1}), Pd/SiO_2-NH_2 (0.0011 s^{-1}) and the other reported catalysts [30, 31], indicating the superior catalytic performance. For a

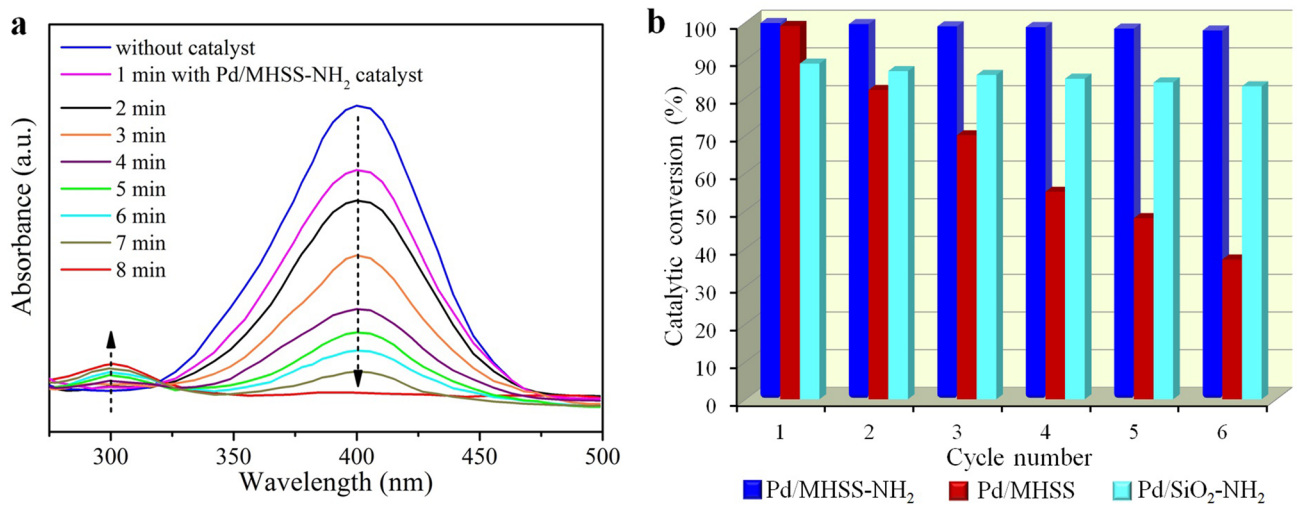

Fig. 6 **a** The UV–vis spectra of reaction mixture recorded with 1 min interval and **b** recyclability of the Pd/MHSS-NH_2, Pd/MHSS and Pd/SiO_2-NH_2 catalysts for the reduction of 4-NP

Table 1 The apparent rate constant (K_{app}) and normalized rate constant (K_{nor}) for the reduction of 4-NP over different catalysts

Sample	C $_{Pd}$ (mM)	K_{app} (s^{-1})	K_{nor} (s^{-1} mM^{-1})	Reference
Pd/MHSS-NH_2	0.0076	0.006	0.79	This work
Pd/MHSS	0.019	0.0043	0.23	This work
Pd/SiO_2-NH_2	0.015	0.0011	0.073	This work
Pd/microgel-PS	0.0022	0.0015	0.70	[30]
Pd/SBA-15 (mesoporous SiO_2)	0.063	0.012	0.19	[31]
Pd-PEDOT-PSS	0.25	0.066	0.26	[34]

quantitative comparison, we introduced the rate constants $K_{nor} = K_{app}/C_{Pd}$, which was defined as the ratio of rate constant K_{app} to the molarity of Pd NPs (C_{Pd}) [32, 33]. The K_{nor} was calculated to be 0.79, 0.23, 0.073 s^{-1} mM^{-1} for the reaction using Pd/MHSS-NH_2, Pd/MHSS and Pd/SiO_2-NH_2 catalysts, respectively. Compared with the reported catalysts [30, 31, 34], the Pd/MHSS-NH_2 exhibited most efficient catalytic activity (Table 1). We considered that the coexisting hollow cavity and mesopores of SiO_2 spheres facilitated reactant molecules to diffuse and subsequently interact with the Pd NPs catalysts.

To explore the practical application, the recycling ability and reusability of the Pd/MHSS-NH_2 were further investigated as demonstrated in Fig. 6b. Recyclability experiments were carried out under the similar reaction conditions (see "Experimental Details" section). In this work, the catalytic conversion of 4-NP to 4-AP is still up to 97.8% even after sixth consecutive runs and exhibited an excellent stability. As expected, Pd/MHSS-NH_2 nanocomposite exhibited a much higher catalytic activity and stability than Pd/MHSS and Pd/SiO_2-NH_2 in the reduction reaction of 4-NP. Firstly, amine groups on MHSS support were beneficial to prevent the aggregation of neighboring Pd NPs. Secondly, the hollow spaces of Pd/MHSS-NH_2 can provide homogeneous micro-environment for the Pd NPs and 4-NP, which greatly improved the catalytic activity and stability. In fact, the moveable core can expose more active sites to interact with 4-NP more effectively.

4 Conclusions

In summary, we described here a simply procedure of preparing amine-functionalized mesoporous hollow SiO_2 spheres (MHSS-NH_2) as support materials to load Pd NPs. The as-prepared catalysts (Pd/MHSS-NH_2) exhibited excellent activity for the catalytic reduction of 4-NP (notorious organic pollutant) under mild conditions. In addition, recyclability experiments demonstrated the stability of Pd/MHSS-NH_2 was satisfying, which was making it a promising candidate for the large-scale industrial application.

Acknowledgements This work was supported by China Postdoctoral Science Foundation funded project (2016M591779), Postdoctoral Science Foundation funded project of Jiangsu province (1601232C) and Modern Agricultural Project of Zhenjiang City (NY2016022).

References

1. Balanta A, Godard C, Claver C (2011) Chem Soc Rev 40:4973–4985
2. Chen Z, Liang Y, Jia DS, Cui ZM, Song WG (2017) Chin J Catal 38:651–657
3. Nagpure AS, Gurrala L, Gogoi P, Chilukuri SV (2016) RSC Adv 6:44333–44340
4. Liu C-H, Lin C-Y, Chen J-L, Lu K-T, Lee J-F, Chen J-M (2017) J Catal 350:21–29
5. Yin H, Tang H, Wang D, Gao Y, Tang Z (2012) Acs Nano 6:8288–8297
6. Hunns JA, Arroyo M, Lee AF, Escola JM, Serrano D, Wilson K (2016) Catal Sci Technol 6:2560–2564
7. Liu X, Zhao X, Zhou M, Cao Y, Wu H, Zhu J (2016) Eur J Inorg Chem 3338–3343
8. Sun X, Zheng Y, Sun L, Su H, Qi C (2015) Catal Lett 145:1047–1053
9. Zhu M, Wang C, Meng D, Diao G (2013) J Mater Chem A 1:2118–2125
10. Liu F, Tian H, He J (2014) J Colloid Interface Sci 419:68–72
11. Cai X, Wang H, Zhang Q, Tong J, Lei Z (2014) J Mol Catal A: Chem 383:217–224
12. Yang X, Liao S, Zeng J, Liang Z (2011) Appl Surf Sci 257:4472–4477
13. Zhao SL, Zhao C, Li XZ, Li F, Jiao LX, Gao WB, Li R (2016) RSC Adv 6:76582–76589
14. Guo M, Li C, Yang Q (2017) Catal Sci Technol 7:2221–2227
15. Ding Y, Sun W, Yang W, Li Q (2017) Appl Catal B 203:372–380
16. Celebi M, Yurderi M, Bulut A, Kaya M, Zahmakiran M (2016) Appl. Catal B 180:53–64
17. Mei X, Yang S, Chen D, Li N, Li H, Xu Q, Ge J, Lu J (2012) Chem Commun 48:10010–10012
18. Braganca LFFPG, Ojeda M, Fierro JLG, Pais da Silva, MI (2012) Appl Catal A 423:146–153
19. Yu P, Zhao X, Li Y, Zhang Q (2017) Appl Surf Sci 393:37–45
20. Liu X, Zhao X, Cao Y, Li T, Qiu S, Shi Q (2017) New J Chem 41:865–872
21. Wang P, Liu H, Niu J, Li R, Ma J (2014) Catal Sci Technol 4:1333–1339
22. Chen Z, Cui Z-M, Cao C-Y, He W-D, Jiang L, Song W-G (2012) Langmuir 28:13452–13458
23. Zhang N, Li G, Cheng Z, Zuo X (2012) J Hazard Mater 229:404–410
24. Ji C.-h., Li J.-j., Hou C.-j., Huo D.-q., Yang M, Zhang L (2017) Sens Actuators B 240:718–725
25. Zhou J, Dong Z, Wang P, Shi Z, Zhou X, Li R (2014) J Mol Catal A: Chem 382:15–22
26. Gu XM, Qi W, Xu XZ, Sun ZH, Zhang LY, Liu W, Pan XL, Su DS (2014) Nanoscale 6:6609–6616
27. Liang Y, Chen Z, Yao W, Wang P, Yu S, Wang X* (2017) Langmuir 33:7606–7614
28. Gu H, Wang JN, Ji YC, Wang ZQ, Chen W, Xue G (2013) J Mater Chem A 1:12471–12477

29. Gu S, Wunder S, Lu Y, Ballauff M, Fenger R, Rademann K, Jaquet B, Zaccone A (2014) J Phys Chem C 118:18618–18625
30. Mei Y, Lu Y, Polzer F, Ballauff M, Drechsler M (2007) Chem Mater 19:1062–1069
31. Morere J, Tenorio MJ, Torralvo MJ, Pando C, Renuncio JAR, Cabanas A (2011) J Supercrit Fluids 56:213–222
32. Long Y, Liu Y, Zhao Z, Luo S, Wu W, Wu L, Wen H, Wang R-Q, Ma J (2017) J Colloid Interface Sci 496:465–473
33. Dong ZP, Le XD, Dong CX, Zhang W, Li XL, Ma JT (2015) Appl. Catal. B 162:372–380
34. Harish S, Mathiyarasu J, Phani K, Yegnaraman V (2009) Catal Lett 128:197–202